Broadband multi-interferometer spectroscopy in high magnetic fields: From THz to visible

W. J. Padilla,[a] Z. Q. Li, K. S. Burch, Y. S. Lee, K. J. Mikolaitis, and D. N. Basov
Department of Physics, University of California at San Diego, La Jolla, California 92093-0319

We present a system capable of broad band frequency domain spectroscopy in the range $6-20\,000$ cm^{-1} at cryogenic temperatures. The apparatus couples two different interferometers to a 9 Tesla superconducting split coil magnet and is designed to work with various detectors, including thermal bolometers and semiconducting detectors. The optical layout utilizes an intermediate focus while preserving optical f/#'s throughout enabling DC magnetic field measurements of small crystals with polarized light in both Voight and Faraday geometries. A reference channel eliminates errors associated with system drift and facilitates determination of the optical constants. For transparent samples, simultaneous reflection and transmission can be performed. © *2004 American Institute of Physics.* [DOI: 10.1063/1.1805252]

I. INTRODUCTION

Spectroscopy is one of the most fundamental and ubiquitous experimental techniques for scientific investigations. For instance, spectroscopy in the infrared regime ($3-30$ THz, $100-1000$ cm^{-1}) is particularly informative due to numerous intrinsic material responses associated with both intra-band electronic transitions, collective modes, and the interaction of radiation with lattice vibrations, i.e., phonons.[1] Many-body electronic effects including density waves[2] and superconductivity[3] also give rise to spectroscopic signatures in the infrared range. There are equally important ranges at lower and higher energies from the infrared region. Currently there is great interest in the lower energy terahertz (THz) range as there are natural absorption bands, due to bio-molecular vibrations,[4–6] as well as biological and chemical agents. As one proceeds higher in energy to the mid and near infrared, there are other various and important electromagnetic signatures associated with vibrational states in organic materials and inter-band transitions in both organic and inorganic solids. A quantitative analysis of optical phenomena in solids relies on a determination of the optical constants.[7] A broad band instrument which covers the above specified ranges is a versatile and invaluable tool. Couple this instrument to a cryostat for temperature dependent measurements and to a high field magnet for magneto-optic measurements and the phase space of properties one can investigate is enormous.

Although investigation of the optical constants in magnetic field is far from new, it is also true that magneto-optical measurements are far from commonplace. Spectroscopy in magnetic fields is technically challenging and has yet to establish itself as a standard routine for scientific exploration. The importance of using magnetic field as a thermodynamically tunable parameter can be summarized by listing some of the phenomena which have been studied. Historically magneto-optical measurements were performed in order to elucidate phenomena such as cyclotron resonance,[8,9] Bardeen–Cooper–Schrieffer (BCS) superconductivity,[10] two-dimensional (2D)-electron gas/ plasmon–phonon interaction, and antiferomagnetic (AF) resonances.[11,12] The importance of magneto-optical measurements has not diminished over the years and currently there is strong interest in: Magnetic semiconductors,[13] metamaterials, strongly correlated systems (field-induced stripes,[14] AF correlations), quantum critical phenomena, electron spin resonance,[15] and high-T_c superconductors. With a demand for devices such as, adaptive lenses, tunable mirrors, isolators, and converters[16] operating at THz frequencies, an ever increasing important characterization of materials is their magnetic properties. As mentioned, a striking example is the recent explosion of interest in diluted magnetic semiconductors (DMS), which has produced great scientific and technological attention in recent years. While these materials hold great technological promise,[17] their broadband magneto-optical response has yet to be fully characterized as appropriate facilities are not numerous. With advances in superconducting magnets it has become feasible to set up large magnetic fields for magneto-optical measurements within an academic institutional laboratory environment.[18–21]

In this article we describe the design and implementation of a magneto-optical spectroscopic system capable of *broadband* high field low temperature measurements. A novelty of the system is the ability to perform absolute measurements of small samples with a good signal to noise. Our research program is aimed at detailed investigations of strongly correlated electron systems, semiconductor superlattices, heavy electron systems and novel superconductors among other magneto-electrodynamic behavior. It is often necessary to go to low temperature and high magnetic fields to elucidate the exotic behavior exhibited by these novel systems.

[a] Present address: Los Alamos National Laboratory, MST-10, MS K764, Los Alamos, NM 87545.
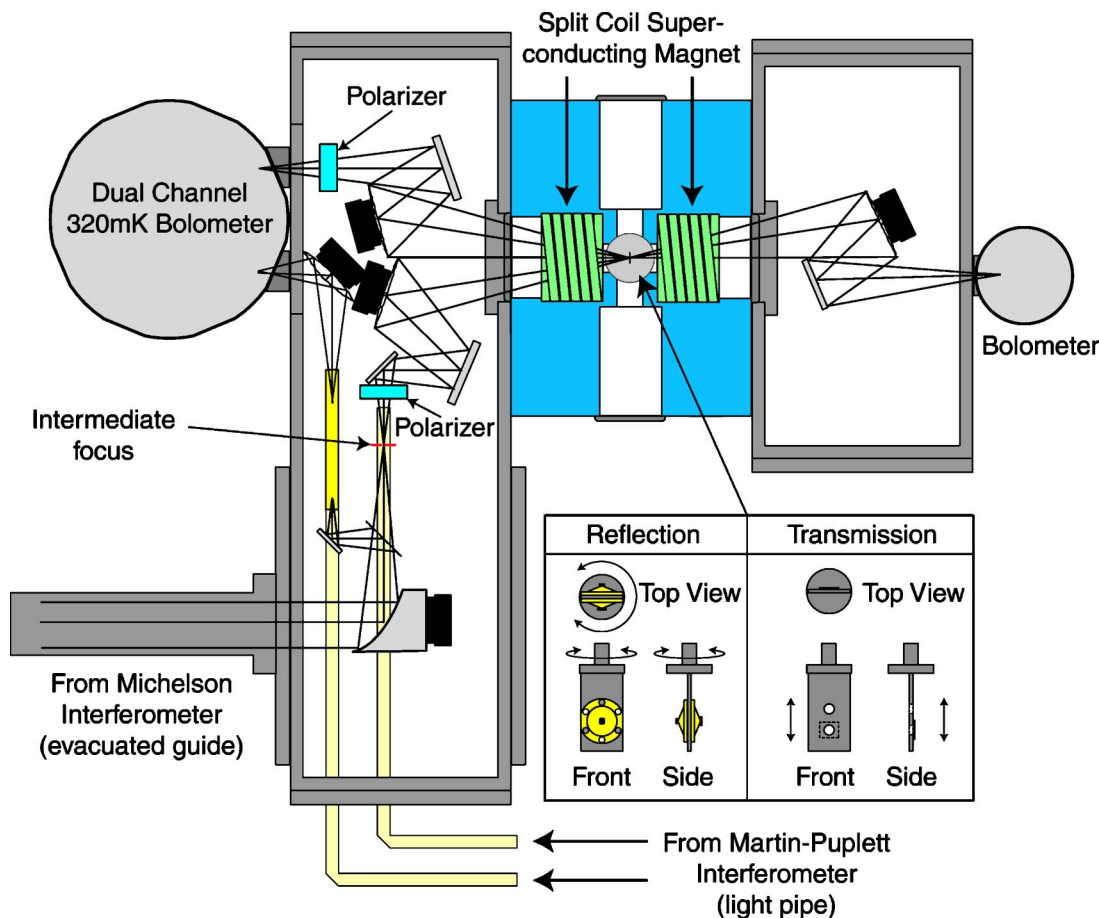
FIG. 1. (Color online) Schematic of the optical layout of an apparatus for absolute measurements of $R(\omega)$ and $T(\omega)$ in magnetic field. Collimated light input from the Michelson interferometer is reflected from a 90° off-axis parabolic mirror with a 8.89 cm focal length. Light then passes through an intermediate focus (shown in red) and off of two flat mirrors before reflecting from the final focusing mirror and into the cryostat. From here the light may then reflect from the sample back into the reflection unit, or continue through to the transmission unit. In both cases the light strikes a focusing mirror then off a flat mirror before impinging upon the detector, here depicted as bolometers. The Martin–Puplett interferometer is coupled by 1/2 I.D. brass pipe depicted as the light yellow segments. The reference channel goes directly to the detector while the sample channel is guided into the same optics used by the Michelson setup. This design allows for a quick change between interferometers by simple removal of the off-axis parabolic mirror, and insertion of the light pipe segments from the Martin-Puplett interferometer. The inset shows two different sample holders used for absolute measurements. In reflection both the sample and a reference mirror are fixed on two cones mounted oppositely. Referenced measurements are thus obtained by rotation of the sample tube through 180°, (depicted in the inset by arrows). In transmission mode the sample is located behind an aperture and reference measurements are obtained by vertical translation (depicted in the inset by arrows) to an open channel. Both methods allow for absolute measurements and are controlled by a stepping motor with encoder feed back. The rotational resolution in reflection mode is 0.02 degrees and the step size in vertical translation is 0.02 mm. The rotational or translational alignment are both highly reproducible and any error in misalignment is within the signal to noise of the system.

II. SYSTEM DESIGN AND COMPONENTS

A. Optics

The heart of the system is a reflectance unit which couples two interferometers to a superconducting magnet, see Fig. 1. This novel design enables the following capabilities: Ability to perform measurements of micro-sized crystals with polarized light, two channel data acquisition, determination of absolute values of both reflectance $R(\omega)$ and transmission $T(\omega)$, and ability to perform broadband spectroscopy. This combination is unique and to the best of our knowledge can only be conveniently implemented with a magnet which uses a split-coil design. It is noteworthy to mention that this optical design yields these significant capabilities without the need for custom magnets or dedicated spectrometers, but allows for a universal system which is usable with many combinations of interferometers or spectrometers and with numerous generic magnetic systems.

While the benefit of most of the above are clear, the advantage of the intermediate focus may be easily overlooked as, for example, commercial systems lack this particular ingredient. Since the interferometer is necessarily located away from the superconducting magnet, the beam travels distances on the order of a meter. As a result the image quality of the beam, even if traveling in an evacuated compartment, is diminished due to scattering and dispersion effects by the time it reaches the sample located within the cryostat. This results in poor image quality on the sample under study and thus in a lower signal to noise due to increased background scattering. A focus within the reflection unit allows one to achieve superb image quality by utilizing an aperture to cut out the scattered light resulting from a long optical path. Thus the improved source image on the sample permits the characterization of small samples. This is an important distinction because many novel and exotic samples

tend to be small when first discovered. Another advantage of the intermediate focus is the ability to measure the magneto-optical permittivities thus permitting determination of the off-diagonal components of the conductivity.[22] The converging beam allows easy placement of a polarizer near the focus and in front of the detector, thus permitting crossed polarized and magneto-ellipsometric measurements.

An additional benefit of the design shown in Fig. 1 is the ability to perform absolute value measurements over a broad frequency range. Although much information can be obtained by analyzing raw transmission $T(\omega)$ or reflectance $R(\omega)$ spectra, the real (χ') and imaginary (χ'') portions of the linear dielectric response of the material enter mixed into both $T(\omega)$ and $R(\omega)$. Thus if the system under study has a complicated electromagnetic response the de-coupling of χ' and χ'' can be quite difficult. The broad-band ability of this instrument allows one to calculate the "optical constants" from $R(\omega)$ or $T(\omega)$ by utilizing the Kramers–Kronig integral relation, which states that if $R(\omega)$ or $T(\omega)$ is measured over all frequencies then by causality, the full complex dielectric function $[\varepsilon(\omega)=\varepsilon_1(\omega)+i\varepsilon_2(\omega)]$, can be calculated. Thus the reference channel shown in Fig. 1, in combination with the broadband nature of the instrument, permit the calculation of the optical constants.

A layout of the optics utilized for the reflection and transmission units, coupled to both the Michelson and the Martin–Puplett instruments, is depicted in Fig. 1. The optics are permanently arranged on bread-boards which sit within the reflection and transmission units and have been designed to work with both interferometers without changing components. This is a big advantage in the set-up time for different experiments. The bread boards are custom made and rest on kinematic mounts.

As mentioned a novelty of the system is the ability to perform referenced measurements utilizing dual channel acquisition. The optical layout depicted in Fig. 1 details how this is accomplished when the unit is connected to both interferometers. The input from the Martin–Puplett interferometer arrives as both a sample channel and a reference channel.[23] The reference channel is then simply directed (with the aid of an internal light pipe segment) to the reference channel on the detector. It is possible to perform referenced measurements using the Michelson interferometer Fig. 2, and in this case, a reference beam is taken from the main input beam and directed to the detector. This is accomplished utilizing a polarizer aligned at 45° to the beam direction and thus no additional loss is incurred for polarized measurements. The advantage of referenced measurement is the ability to compensate for: Magnetic field effects on the interferometer or source, light source instability, and system drift during long acquisition times. These issues are primarily relevant for spectroscopy in the far infrared regime (FIR) regime and thus a light pipe is suitable for the reference channel.

After light traverses from each interferometer through either the light pipe or the evacuated compartment it then exits into the reflection unit. Note that the light entering into the reflection unit, from either the light pipe or evacuated guide, is unpolarized. Thus a polarizer is used within the

FIG. 2. (Color online) Photograph of the 9 Tesla superconducting magnet connected to the Michelson interferometer. The units are connected by 750 cm of evacuated guide. The platform is where the detector would sit for reflection experiments. A similar box sits on the opposite side of the magnet for transmission (not shown).

reflectance unit for measurements of anisotropic samples. Both the reflection and transmission units have been constructed from a solid piece of aluminum and fabricated on a digital mill. The cost of such a procedure is approximately 10% more than had the units been constructed from welded flat aluminum plates. However, the advantage of this design is that it yields a more robust unit with relatively thin walls, which is capable of being evacuated. The boxes sit on three legs and have various flanges and ports built in on all sides for versatility. A black hard anodized finish is applied to the boxes ensuring a long lifetime for parts which are frequently bolted and unbolted, and additionally minimizes reflections. A lid sits atop the boxes and seals with an O-ring gland.

B. Interferometers

As mentioned the system couples the output of two interferometers, with overlapping frequency coverage, to a superconducting magnet. The interferometers are a Fourier transform (Michelson) interferometer and a Martin–Puplett (MP) interferometer. The Michelson interferometer is a commercially available Fourier transform unit [Bruker IFS 66v/S Vacuum Fourier transform infrared (FT-IR)] capable of measurements in a broad range (20–25 000 cm^{-1}, 0.6–750 THz, 2.48 meV–3 eV) with a maximum resolution of 0.25 cm^{-1} =7.5 GHz (apodized). This interferometer uses light sources such as a mercury (Hg) arc lamp, SiC globar, and tungsten lamp. Mercury is utilized primarily in the THz and infrared region, globar in the infrared and MIR regimes, and tungsten
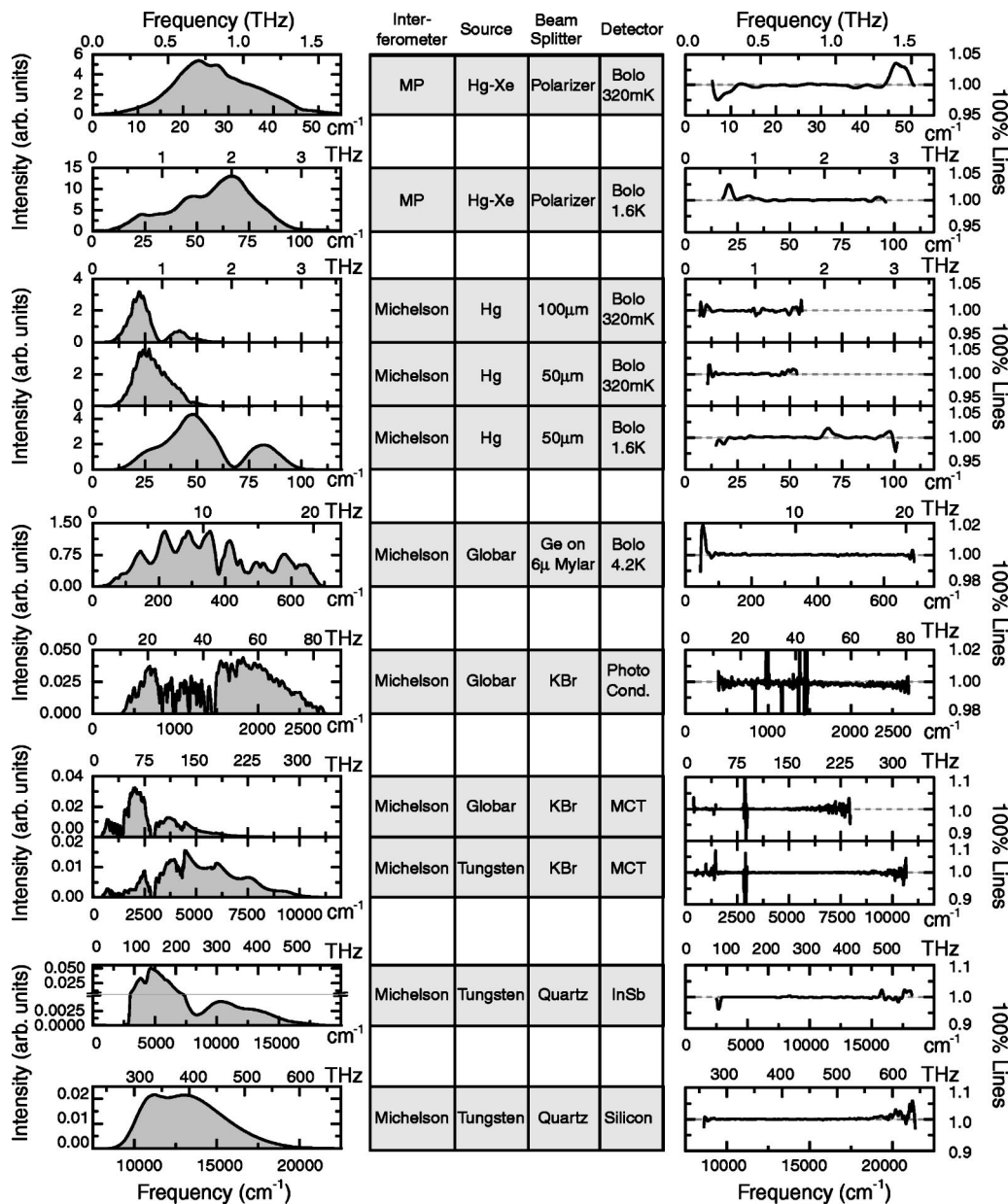
FIG. 3. Power spectrum, configuration, and 100% lines in reflectance mode. The left panels depict the intensity of several configurations plotted vs. frequency, the middle panels show the configuration used for these spectra, and the corresponding 100% lines for each spectrum are presented in the right panels The top two rows are for the MP setup and the remaining are with the Michelson interferometer. The panels are presented from lowest frequency (THz range in top panel) to highest frequency (Optical in bottom panel). All components used for these measurements are listed in the middle panels.

in the MIR through optical frequency ranges. Several different beam splitters are used for various ranges, see Fig. 3.

The Martin–Puplett interferometer has an unapodized maximum resolution of 0.06 cm^{-1}=1.8 GHz, is designed to work in the lower sub-THz and mm-wave region of the spectrum (1–100 cm^{-1}) and is based on a Sciencetech 200 instrument. The Martin–Puplett interferometer is used in the low frequency regime because of its higher resolution and greater sensitivity (a factor of 3 in the sub-THz regime) over that of the Michelson interferometer (see Fig. 3). A 150 watt Mercury–Xenon arc lamp (Hamamatsu photonics L2482) is used for a source. The Martin–Puplett design utilizes a wire grid polarizer rather than beam splitters as in the Fourier transform setup. This allows for nearly perfect beamsplitter efficiency, even at frequencies of 200 GHz (~7 cm^{-1}). All

components of the interferometer are assembled on an optical breadboard and are housed in a vacuum compartment to avoid strong absorption in THz range at ambient conditions. The Martin–Puplett interferometer is a step-scan instrument and thus acquisition times can be quite long, ~5–20 min. Thus the outgoing polarizer is also used as a beam splitter to split off a reference beam from the main channel. This allows one to collect accurate measurements through the use of a second channel in conjunction with a two channel detector, described previously in detail.[23]

C. Evacuated guide and light pipes

The coupling of both the Martin–Puplett and the Michelson interferometer to the reflection unit is performed with

both evacuated light guides (a compartment in which the collimated beam travels) and by conventional light pipes. Light pipe segments are ideal and easily handled however the multiple reflections and properties of the light pipe do not permit their use at high frequencies.

In the case of the Michelson interferometer, collimated light is internally reflected from a computer controlled motorized mirror to a port located on the side of the instrument. From here the light passes through an evacuated compartment to the reflection unit. This method is preferred since the light makes no internal reflections within the evacuated guide, and loss is minimized thus permitting measurement up to optical frequencies. The coupling to the Michelson interferometer is performed through standard ASA fittings, i.e., a cylindrical segment with O.D. 3″. The utilization of these standard O-ring sealed components allows different segments to be used to vary the distance of the Michelson interferometer to the magnet, which may be important to minimize magnetic field effects on the spectrometer and light source. We have found that an evacuated guide length of 750 cm is suitable to minimize magnetic effects on the spectrometer, while preserving the quality of the collimated beam.

For the Martin–Puplett instrument conventional light pipes are used, since light at these frequencies is extremely long wavelength. New copper pipe, (½″ I.D.), readily available form any hardware store is used where the interior is not polished or plated. Light from the sample and reference channel exiting from the Martin–Puplett interferometer is focused into the opening of the light pipe. Due to the particular arrangement of equipment it was necessary for the light pipes to make one or more 90° bends before entering the reflection unit. This has been accomplished by constructing 90° elbows that attach to the light pipe and are sealed with o-ring flanges. The ideal geometry to use for such a turn is in-fact an ellipsoidal mirror with the light pipe terminating at a specific distance (depending on the f/# of the instrument) beyond the focus of the ellipse. However, the 90° elbows are very simple and easy to implement and end up reducing the intensity of light by ~20% per elbow.[24]

D. Superconducting magnet

The magnet used here is a 9 Tesla superconducting split coil magnet made by Oxford (Spectromag SM-9000). The particular arrangement of the coils is depicted in Fig. 1. The split coil design allows both measurements with the magnetic field parallel to the propagation vector (k) called Faraday geometry and perpendicular to k Voight geometry. The system we have designed is readily compatible with many split coil magnets offered by various vendors including those with higher maximum fields.

The design of the magnet requires two windows for the light to pass through before making it to the sample. A room temperature window, and a liquid helium window ($T=4.2$ K) mounted on the variable temperature insert (VTI). Both the 300 K and LHe windows are made from 50 μm thick transparent polypropylene. A big advantage of the polypropylene utilized here is the transparency of the windows to visible light which is ideal for alignment of the samples.

Two custom sample holders have been designed to attach to the supplied sample tube (see inset to Fig. 1), one for reflectance and the other for transmission measurements. The reflectance sample holder is constructed such that two samples can be mounted, thus a reference mirror can be mounted in addition to the sample and absolute reflectance values can be obtained. The sample and the reference are mounted on a reflective cone which is attached to the sample mount. The cones allow one to study a sample physically smaller than the spot focus since only light that is specularly reflected from the surface of the sample is collected by focusing optics and sent to the detector, while light reflected by the cone does not. The custom transmission sample holder allows for referenced measurements by vertical translation to an open channel, (aperture). The repositioning of both the reflection and transmission sample holders is accomplished with a stepping motor attached to the top of the sample tube with encoder feedback. An enclosure for the stepping motor made of high permeability mu metal allows its use over the full range up to 9 Tesla. Both of the custom sample holders are depicted in the inset to Fig. 1.

III. ZERO FIELD CHARACTERIZATION

We have characterized the system performance in a number of different configurations. In each particular setup the components are optimized for a particular frequency range and the electronic gain is identical for bolometers. One component common to all data presented is the windows used on the superconducting magnet, which is polypropylene in this case. The results from these tests are displayed in Fig. 3.

An indicator of the quality of a spectroscopic system is encapsulated within the power spectrum. This is depicted in the left panels of Fig. 3 for each configuration. For bolometers the optical cutoffs are determined by cold ($T=77$ K, and $T=4.2$ K) filters installed within the detectors. The frequency dependent fluctuations are intrinsic to each arrangement and are due to interference fringes related to the thickness of the beam splitter. The mid-infrared (MIR) spectrum exhibits frequency dependence and the intensity has several minimums. These are associated with five absorption lines (in this range) due to the polypropylene windows used for all experiments. The reduced intensity associated with these lines is very manageable as the bandwidth is narrow. The advantage of the polypropylene windows is the large frequency range over which it can be used. Usually this is of little concern as the frequency dependence of samples characterized in transmission or reflection within this range is small and thus this is a suitable tradeoff.

Another typical measure of a spectroscopic system is a so-called 100% line. This gauge is obtained by measuring either a transmission or reflectance spectrum and then dividing by a subsequent spectrum. Thus the division of these two should be a straight line at 100% and deviations from this represent the noise and instability of the system. 100% lines for numerous configurations are displayed in the right col-

umn of Fig. 3. This parameter displays the noise as a function of frequency and thus the relative error bars for all energy ranges can be characterized.

These gauges of the zero field performance have been done in reflectance mode. The performance of the unit in transmission mode is not shown, but typically both the power spectrum and 100% lines are significantly enhanced. Another relevant comparison is to that of the zero field interferometer performance when connected directly to the various detectors. We have found that the magneto-optical system presented here has a reduction in intensity of approximately 50% in reflectance mode compared to that of the original systems. This is a reasonable reduction considering the added optical length, addition of extra optical components, and double the number of cryostat windows.

IV. MAGNETO-OPTICAL MEASUREMENTS

A. Reflectance mode

As a gauge of the magneto-optical system in reflection mode we have chosen graphite and $YBa_2Cu_3O_y$ (YBCO) as two canonical samples to measure. Although there has been a large amount of work done on graphite,[25] there has yet to be a systematic investigation of the optical constants at various magnetic fields and temperatures. Additionally the development of intra-band and inter-band transitions in magnetic fields is unexplored. As for high-T_c superconductors, one of the most important unresolved issues is the exact role of the spin resonance in superconducting properties.[26,27] It is also not clear how the spin resonance is relevant to the optical conductivity. YBCO is one of the most appropriate systems for this issue because of the many systematic studies on the spin resonance. However, there are not many studies of the magneto-optical properties of YBCO, possibly due to the limiting factor imposed by small sample size.

The particular graphite sample characterized is a so-called highly oriented pyrolytic graphite (HOPG). The dimensions of the ab plane surface characterized in reflectance measurements are $\sim 6 \times 6$ mm^2. With our unique instrument, we are able to measure the reflectance of graphite at various temperatures and magnetic fields up to 9 Tesla in a broad frequency range. The magneto-optical measurements were performed from 5 to 3000 cm^{-1} at temperatures between 4.2 K and room temperature. For comparison, measurements were also completed from 5 to 50 000 cm^{-1} at zero field.

In order to obtain the optical constants of graphite, we combined reflectance data in magnetic fields below 3000 cm^{-1} and zero field reflectance data above 3000 cm^{-1}. This is warranted since the reflectance spectra have no observable magnetic field dependence as one approaches ~ 3000 cm^{-1}. The data was then extrapolated to low frequency using the standard Drude form and to higher frequencies using the free electron model. A Kramers–Kronig (KK) transformation of the data then allows us to obtain the optical constants. Various different extrapolations to low frequency were used and verify that the particular method produced no noticeable effects of $\sigma_1(\omega)$ over the measured frequency range.[1] Therefore, by KK transformation of the reflectance
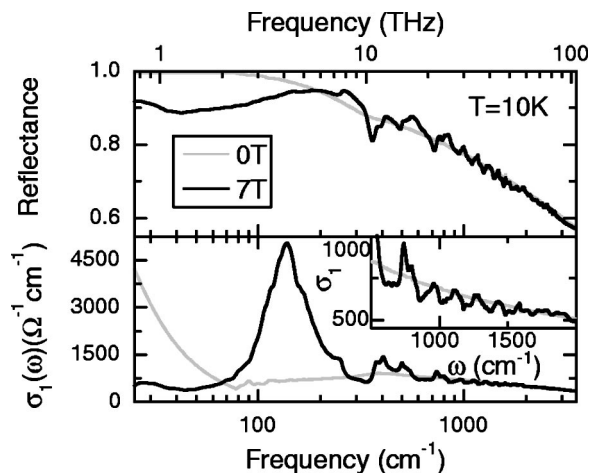

FIG. 4. Top panel: Reflectance of graphite (HOPG) at 0 and 7 Tesla, both at 10 K. Bottom panel: Real part of the optical conductivity $\sigma_1(\omega)$ obtained by Kramers–Kronig transformation of the reflectance data in the top panel. The bottom inset shows the detailed peak structures of $\sigma_1(\omega)$ in the MIR region, which are due to the inter-band transitions between Landau levels in magnetic fields. The reflectance at field was obtained by the Martin–Puplett spectrometer, with a 320 mK bolometer from 5 to 50 cm^{-1} and with a 1.6 K bolometer from 20 to 110 cm^{-1}. The Michelson interferometer, with a 4.2 K bolometer, was used from 70 to 700 cm^{-1}, and with a photoconductor detector from 400 to 3000 cm^{-1}. The data in NIR region above 3000 cm^{-1} were measured by the Michelson interferometer with an InSb detector and a grating spectrometer in the UV region up to 50 000 cm^{-1}.

data, we are able to obtain the real part of the optical conductivity of graphite at all fields and temperatures up to about 3000 cm^{-1}, with good accuracy.

In the zero field case, a conventional KK analysis assumes time reversal symmetry. However, in the presence of magnetic fields, time reversal symmetry is broken and a modified form of the KK relations has to be used.[28] This latter form includes off-diagonal components of the response function tensor, e.g., σ_{xy}. To characterize the off-diagonal components σ_{xy}, the maneto-optical Kerr effect was investigated up to 8 T using two 90-degree crossed polarizers and no effect was found throughout the entire infrared region. This can be understood from the special properties of the Fermi surface of graphite.[29] Due to the distorted Fermi surface, electrons can be partially accelerated by both left- and right-handed circularly polarized light, and the same for holes. This fact, together with the equal density of electrons and holes, results in a very small rotation of polarization, i.e., negligible σ_{xy}. Therefore, the optical constants of graphite in magnetic fields can be obtained by a conventional KK transformation directly.

As an example, Fig. 4 shows the reflectance spectrum $R(\omega)$ and the corresponding $\sigma_1(\omega)$ spectrum of graphite at $H=0$ T and $H=7$ T, both at 10 K. In $\sigma_1(\omega)$ at zero field (grey curve bottom panel of Fig. 4), a Drude component is observed below 100 cm^{-1}, which is due to the intra-band transition in graphite. In the MIR region (from 100 cm^{-1} to 1000 cm^{-1}), there is a broad absorption peak due to the inter-band transition of the π bands. Notably at fields of 7 Tesla field there is no Drude component centered at zero frequency. Instead, the free carrier absorption is shifted to a finite energy resonance (from 100 to 300 cm^{-1}), i.e., cyclotron resonance, by the magnetic field. The energy bands of
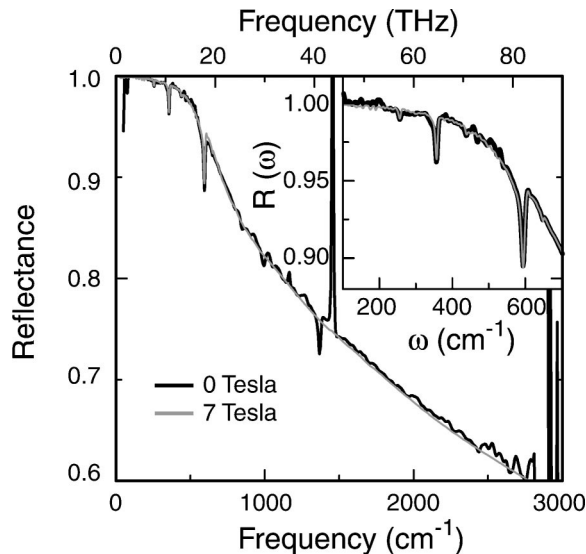
FIG. 5. Reflectance spectra of $y=6.65$ YBCO. There are no significant differences between the zero field and high field values of the reflectance for all frequencies measured. The inset shows a detail of the infrared region.
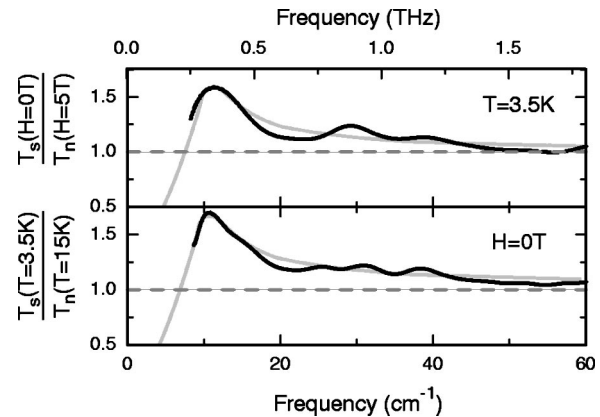

FIG. 6. Top panel: Ratio of the transmission in the superconducting state at zero field to that of the transmission at 5 Tesla. Bottom panel: Ratio of the superconducting transmission at 3.5 K to that at 15 K.

graphite are split into different Landau levels and the peaks of $\sigma_1(\omega)$ in the MIR region at 7 Tesla are a signature of the interband transitions between these levels. It is worth pointing out that the spectra of graphite show field dependences up to energies as high as ~2500 cm$^{-1}=310$ meV. This unique instrument permits measurements in large magnetic fields continuously over frequencies from 5 cm^{-1} up to 3000 cm^{-1}, thus enabling us to systematically investigate these interesting high energy phenomena.

An experimental challenge of the YBCO crystal measurements is their relatively small size 1.0×1.2 mm^2 compared to the large graphite crystals. Thus a characterization of YBCO was undertaken also to verify the sensitivity of the instrument for small samples. The samples were measured and referenced with respect to a perfect reflector, i.e., a mirror. The samples were then coated with gold and then the referenced measurements were repeated. Then a ratio of the two of these measurements (double ratio) allows a determination of absolute values for small sample sizes, and has been described previously.[30]

YBCO is a high temperature superconductor with a maximum $T_c\sim95$ K at the so-called "optimal doping" of $y=6.95$. For underdoped YBCO, the system exhibits a spin resonance at approximately 34 meV.[31] Additionally the reflectivity is nearly unity due to the superconducting response and/or high conductivity. Thus a characterization of the magnetic field dependence of this effect is challenging.

In Fig. 5 we show two reflectance spectra of $y=6.65$ YBCO which has a critical superconducting temperature of $T_c\sim60$ K. The data were obtained in the polarization E∥a and, therefore, represent the genuine response of the CuO$_2$ planes without a contribution of the Cu−O chains running along the b-axis. The figure shows $R(\omega)$ at zero field and also at 7 Tesla. Notice there is no difference, within experimental error, between the two spectra over frequencies at least up to 3000 cm^{-1}. The inset is a detail of the reflectance spectra with a span of about 10%. The abrupt decrease near

500 cm^{-1} is referred to as the "knee,"[32] and has been considered to be relevant to the spin resonance.

According to neutron scattering experiments, the intensity of the spin resonance should be reduced by about 30% at $H=6.8$ T.[31] So, one can expect that the knee structure should be suppressed with magnetic field. However, there is no observable effect at fields up to 7 T as our model calculations show.[33] The small changes observed in the spectra are within the noise level of the instrument, $\sim1\%$ in the FIR regime for small crystals. So, it appears that the optical conductivity does not couple to the spin resonance, the effect lies lower in frequency, or the effect is smaller than expected.

B. Transmission mode

Niobium (Nb) is a BCS superconductor with a bulk superconducting temperature of $T_c\sim9.5$ K and a critical field of $H_c\sim0.2$ T. For thin films of Nb the dependence of T_c vs film thickness has been characterized and found to be strongly reduced for thicknesses below about 100 A. Figure 5 shows transmission spectra of a Nb thin film with a thickness of 120 A on a 50 μm sapphire substrate grown at the University of California, San Diego. The sample has a T_c of 9.2 K and the measurements were performed with the Martin–Puplett interferometer at a resolution of 3 cm^{-1} and a scan time of four minutes. The interferometer was coupled to the reflection unit through 10 feet of ½″ brass light pipe and undergoes one 90° bend. After light passes through the focusing optics it impinges upon the sample and then into the transmission box and finally to the detector, (see Fig. 1). The detector used for collection of the data was a thermal bolometer designed for use at 1.6 K.

The data is displayed as transmission ratios of the superconducting state divided by the normal state, $T_s(\omega)/T_n(\omega)$. In the top panel the normal state is obtained by increasing the magnetic field beyond the critical value H_C, while in the bottom panel the normal state is obtained by raising the temperature above the critical temperature T_c. In both curves a strong enhancement of the transmission spectra occur do to superconducting state. In the theory of Mattis–Bardeen, the spectra should peak at an energy of 2Δ which is about $2\Delta=15$ cm$^{-1}=1.86$ meV in these samples. The form of the

thin film interference exhibited by the substrate is responsible for the slight disagreement between the fits to the data displayed in Fig. 6. However, the agreement between both spectra is evident[34] thus suggesting that the particular manner in which the normal state is obtained is not relevant.

ACKNOWLEDGMENTS

[1] F. Wooten, *Optical Properties of Solids* (Academic Press, New York, 1972).

[2] G. Gruner, *Density Waves in Solids* (Perseus Publishing, Massachusetts, 1994).

[3] D. N. Basov and T. Timusk, Rev. Mod. Phys. (In Press).

[4] A. Markelz, A. Roitberg, and E. Heilwiel, Chem. Phys. Lett. **320**, 42 (2000).

[5] M. Walther, B. Fischer, M. Schall *et al.*, Chem. Phys. Lett. **332**, 389 (2000).

[6] T. R. Globus, D. L. Woolard, A. C. Samuels, B. L. Gelmont, J. Hesler, T. W. Crowe, and M. Bykhovskaia, J. Appl. Phys. **91**, 6105 (2002).

[7] An accurate determination of the optical constants by a Kramer–Kronig transformation requires a measurement of transmission or reflection over all frequencies. See Ref. 1.

[8] G. Dresselhaus, A. F. Kip, and C. Kittel, Phys. Rev. **92**, 827 (1953); Phys. Rev. **98**, 368 (1955).

[9] Benjamin Lax, H. J. Zeiger, R. N. Dexter, and E. S. Rosenblum, Phys. Rev. **93**, 1418 (1954).

[10] M. Tinkham, *Introduction to Superconductivity*, 2nd ed. (McGraw-Hill, New York, 1996).

[11] F. M. Johnson and A. H. Nethercot, Jr., Phys. Rev. **104**, 847 (1956).

[12] Edward S. Dayhoff, Phys. Rev. **107**, 84 (1957).

[13] S. S. A. Seo, M. W. Kim, Y. S. Lee, T. W. Noh, Y. D. Park, G. T. Thaler, M. E. Overberg, C. R. Abernathy, and S. J. Pearton, Appl. Phys. Lett. **82**, 4749 (2003).

[14] B. Lake, H. M. Rønnow, N. B. Christensen, G. Aeppli, K. Lefmann, D. F. McMorrow, P. Vorderwisch, P. Smeibidl, N. Mangkorntong, T. Sasagawa, M. Nohara, H. Takagi, and T. E. Mason, Nature (London) **415**, 299 (2002).

[15] László Mihály, Diyar Talbayev, László F. Kiss, Jianshi Zhou, Titusz Fehér, and András Jánossy, Phys. Rev. B **69**, 024414 (2004).

[16] V. Zayets, M. C. Debnath and K. Ando, Appl. Phys. Lett. **84**, 565 (2004).

[17] S. A. Wolf, D. D. Awschalom, R. A. Buhrman, J. M. Daughton, S. von Molnar, M. L. Roukes, A. Y. Chtchelkanova, and D. M. Treger, Science **294**, 1488 (2001).

[18] S. V. Dordevic, Seiki Komiya, Yoichi Ando, and D. N. Basov, Phys. Rev. Lett. **91**, 167401 (2003).

[19] Y. Okimoto and Y. Tokura, J. Supercond. **13**, 271 (2000).

[20] A. Perucchi, L. Degiorgi, J. Jun, M. Angst, and J. Karpinski, Phys. Rev. Lett. **89**, 097001 (2002).

[21] K. M. Kojima, S. Uchida, Y. Fudamoto, and S. Tajima, Phys. Rev. Lett. **89**, 247001 (2002).

[22] S. Spielman, B. Parks, J. Orenstein, D. T. Nemeth, F. Ludwig, J. Clarke, P. Merchant, and D. J. Lew, Phys. Rev. Lett. **73**, 1537 (1994).

[23] D. N. Basov, S. V. Dordevic, E. J. Singley, W. J. Padilla, K. Burch, J. E. Elenewski, L. H. Greene, J. Morris, and R. Schickling, Rev. Sci. Instrum. **74**, 4703 (2003).

[24] D. G. Hawthorn and T. Timusk, Appl. Opt. **38**, 2787 (1999).

[25] For a current review see, N. B. Brandt, S. M. Chudinov, and Ya. G. Ponomarev, *Semimetals: 1. Graphite and its Compounds* (Elsevier Science publishing, New York, 1988); B. T. Kelly, *Physics of Graphite* (Applied Science, London, 1981).

[26] Pengcheng Dai, H. A. Mook, S. M. Hayden, G. Aeppli, T. G. Perring, R. D. Hunt, and F. Doğan, Science **284**, 1344 (1999).

[27] Pengcheng Dai, H. A. Mook, R. D. Hunt, and F. Doğan, Phys. Rev. B **63**, 054525 (2001).

[28] D. Y. Smith, J. Opt. Soc. Am. **66**, 454 (1976).

[29] M. Inoue, J. Phys. Soc. Jpn. **17**, 808 (1962).

[30] C. Homes, M. A. Reedyk, D. A. Crandels, and T. Timusk, Appl. Opt. **32**, 2976 (1993).

[31] P. Dai, H. A. Mook, G. Appeli *et al.*, Nature (London) **406**, 965 (2000).

[32] N. L. Wang, T. Timusk, J. P. Franck *et al.*, Phys. Rev. Lett. **89**, 087003 (2002).

[33] Y. S. Lee, unpublished.

[34] A. V. Pronin, M. Dressel, A. Pimenov, A. Loidl, I. V. Roshchin, and L. H. Greene, Phys. Rev. B **57**, 14416 (1998).